International Journal of Innovation Scientific Research and Review
Vol. 05, Issue, 04, pp.4301-4307, April 2023
Available online at http://www.journalijisr.com
SJIF Impact Factor 2023: 6.599

IJISRR

ISSN: 2582-6131

Research Article

DEVELOPMENT OF AN ENTRY-LEVEL ROBOTIC PROSTHETIC FOOT SUPPORTED BY THE TOE AND METATARSAL BONES

Dr. Su-Chak Ryu, Dr. Joon-Hyub Kim, Sung-Kwang Jo, * Seung-Hyeon Kim

School of Nanomechatronics Engineering, Pusan National University, Pusan, 46241, Korea.

Received 05th February 2023; Accepted 06th March 2023; Published online 12th April 2023

ABSTRACT

this study, a bio-inspired design was introduced to fabricate an inexpensive robotic prosthetic foot. Toe joints and torsion springs improve gait stability and propulsion. Additionally, the metatarsal design shifts the power point from the tip of the toe to the head of the metatarsal bone, reducing the strength of the material required. Measurements showed a tensile strength of 602.0 MPa. A finite element analysis was performed for the toe-off situation, and the validity of the material with a tensile strength of 33.23 MPa and a safety factor of 3.02 or more was proven at the part where the most stress occurred. To recognize the gait phase, a pressure sensor was used to detect foot contact with the ground. As a result of comparing the results of the gait recognition test with the acupressure change data when a person is walking, similar FSR responses to acupressure were shown at each location. Finally, it showed the possibility of providing an entry-level robotic prosthetic foot at a manufacturing price of $500.

Keywords: Robot prosthesis foot, Metatarsals bone head, Toe joint, FSR sensor, Bio-inspired.

INTRODUCTION

worldwide, amputees need prosthetic feet because of accidents, diseases, wars, etc. In the United States, the number of lower extremity amputations is estimated to be 2 million, and it is expected to increase by 187,000 annually [1, 2]. Even though nonrobotic prosthetic feet are widely used because they are affordable, walking naturally is difficult. To solve this problem, robotic prosthetic feet have been developed. The muscle electrical signal or gyro signal of the user provides ankle rotation according to the gait, enabling the user to walk more naturally. However, these feet are not affordable to everyone. Therefore, this study proposes an ergonomic design of affordable robotic prosthetic feet, which mimics the toe joint and metatarsal head, and recognizes the gait phase by sensing ground pressure.

DESIGN CONCEPT

A. Biomechanics of the human foot

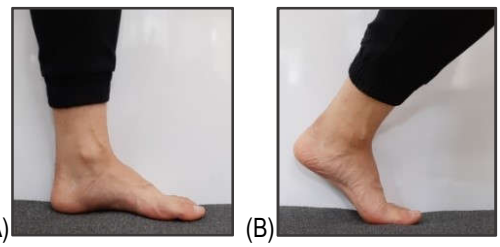

Fig. 1 Two types of foot shapes while walking, (A) the shape of a flat foot before the Heel Off. (B) The shape of the bent foot after the Heel Off, and before the Toe Off

***Corresponding Author: Seung-Hyeon Kim,**
School of Nanomechatronics Engineering, Pusan National University, Pusan, 46241, Korea.

As shown in Fig. 1, there are two types of foot shape when walking. From Heel Strike (HS) to Foot Flat (FF), the foot is flat as shown in Figure 1(A). The foot flexes from Heel Off (HO) to Toe Off (TO) as shown in Figure 1(B). Bent feet are formed based on the toe joints, and the toes touch the ground and function for walking. The function of the toe is to smoothly move the Zero Moment Point (ZMP) between Single Support Pose (SSP) and Double Support Pose (DSP) to minimize fatigue in the ankle, knee, and hip joints. This increases stroke length and improves energy efficiency [3-6]. In the case of bipedal robots without toes, ZMP moves differently from human walking, so joints are excessively bent, resulting in instability and increased fatigue [7-9]. However, many robot feet equipped with toes concentrate all the load on the toe during TO, increasing the risk of fracture [10-21]. To prevent breakage, the forefoot is not properly loaded with weight. So ZMP moved quickly like a toeless robot foot when moving from DSP to SSP. Therefore, many studies have applied toes to robotic feet. However, the effect is minimal. In this study, we propose a design that applies the toe and metatarsal head surfaces. In addition to the advantages of the toe, the metatarsal head is designed to be inclined, so when the foot is bent during walking, the load is applied to the slope, not the toe. In addition, by utilizing the face of the head of the metatarsal bone, an FSR (Force Sensing Resistor) sensor was attached to this face so that the robot prosthesis can recognize the gait phase. It infers gait steps and measures speed and incline to improve gait. The goal of this study is to develop a robotic prosthetic limb that provides comfortable walking while reducing the economic burden of lower limb patients.

B. Forefoot design

It is a 3D model of the forefoot as shown in Fig. 2(A). The white parts are the two toes, one on each side of the metatarsal. The pink and red planes correspond to metatarsal and metatarsal slopes, as shown in Fig.2(B). The metatarsal and toe parts are fixed with bolts and can be rotated around the axis of the bolt. One torsion spring is mounted on each side between the metatarsal bone and the toes.

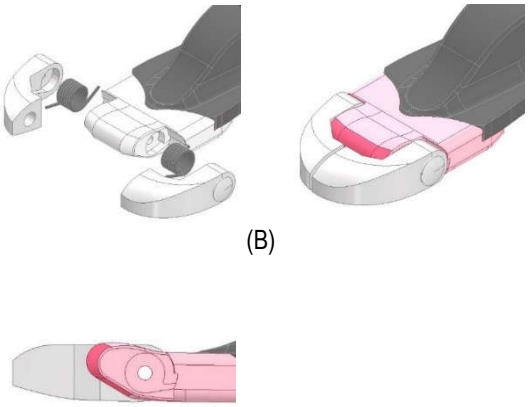

(A) (B)

(C)

Fig. 2 Forefoot design of a robotic prosthetic foot: (a) full assembly, (b) torsion spring exploded view, and (c) sagittal cross-sectional view of the metatarsal bone head slope

Each torsion spring stores torsional elastic energy according to toe extension action. At the end of the TO, elastic energy is released to propel the wearer. An appropriate torsion spring is calculated when a 70 kg adult male wears a robotic prosthesis. The load applied to the toe during TO during walking is BW × 24% [22]. Therefore, when a load is applied to the torsion spring, the load applied to each torsion spring is (BW×24%)/2, which is 82.32 N. Table 1 shows the specifications of the torsion spring used in the robotic prosthetic leg developed in this study. A piano wire material torsion spring with high strength and good homogeneity is used for a robotic prosthesis, where E is the longitudinal modulus of elasticity, d is the wire diameter, D is the outer diameter, Nt is the total number of turns, and a1 and a2 are the arm lengths. A sagittal section of the robotic prosthesis is shown as in Fig 2(C). The slope is 30° from the ground. This is for the metatarsal slope to contact the ground with ankle rotation and toe extension during TO. From the HS stage to the FF stage, the metatarsal slope does not contact the ground, and from the HO to the TO, the load is endured by contacting the ground during toe extension.

TABLE I

TORSION SPRING SPECIFICATIONS USED FOR THE ROBOTIC PROSTHETIC FEET

Option	Value
E (kg/mm^2)	21000
d (mm)	2
D (mm)	20.5
Nt	3
a1 (mm)	15
a2 (mm)	15

C. Mechanical design

As shown in Fig. 3(A), it shows the robotic prosthetic foot model used in this study. The metatarsals and toes are in the forefoot, while the motor and gearbox used to move the heel and ankle joints are in the hind foot. The battery MPU is located above the ankle. In this study, an electric motor is used instead of a hydraulic or pneumatic cylinder to move the ankle joint. Hydraulic and pneumatic cylinder actuators are difficult to maintain and require complex control valve designs. Servo motors are chosen because of their stable control, low noise, and excellent environmental resistance. The motor used in this study is CYS-S1100 (CYS Model Technology Co. Ltd). Table 2 shows the specifications of the motor. Ankle torque required for a robotic prosthesis to support human walking is 130 N·m [23, 24]. In this study, the motor torque required for a robotic prosthesis can be reduced by 47% due to the shift of the force point of the metatarsal and toe design [25]. The rotational torque applied to the ankle joint for plantar flexion during the TO step is 61.1 N·m.

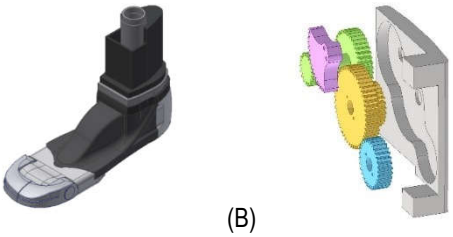

(A) (B)

Fig. 3 Forefoot design of a robotic prosthetic foot: (a) full assembly, (b) torsion spring exploded view, and (c) sagittal cross-sectional view of the metatarsal bone head slope

TABLE II

THIS SPECIFICATIONS OF CYS-S1100 Motor

Option	Value
Weight (g)	274
Size (mm)	79.8 × 30 × 64.35
Operating Voltage (V)	9.0~12
Operating Speed (sec/60 °)	0.40(9V)~0.3(12V)
Stall Torque (kg · cm)	90(9V)~110(12V)

As shown in Fig. 3(B), there is a gearbox inside the robot prosthesis. It is composed of two-stage spur gears, and the final reduction ratio of the gearbox is 7:1. The torque of the motor required to move the ankle of the robot prosthesis is 8.73 N·m due to the reduction ratio of the gearbox.

D. Control system design

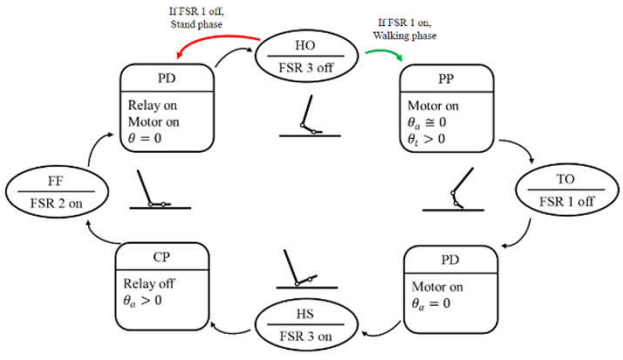

Fig. 4 Finite-state machine for walking steps

In Fig. 4, a finite state machine is implemented to control the motion of a robotic prosthetic limb suitable for the walking phase. Ankle rotation is driven by a motor, and each step is recognized by a Force Sensitive Resistor (FSR) sensor located on the sole. In this study, FSR sensor is used. The gyro sensor used in existing robotic prostheses has the disadvantage of drifting due to accumulation of

errors when integrating and digitizing the measured angular velocity information. Since the walking motion is repetitive, it is highly likely that the error value has been accumulated. Also, due to the structure of the human body, each person has a different leg angle. Therefore, additional costs are incurred in the customization process. Another sensor used in robotic prostheses is the electromyographic (EMG) sensor. The process of applying a water-based gel to the body to better accommodate the electrical signals of the muscles makes the wearer uncomfortable. The FSR sensor was comfortable even when attached to the sole of the foot due to its simple structure and mechanical characteristics. Moreover, it is not affected by the body type characteristics of the user. Therefore, since the price is low, it is judged to be in line with the concept of an entry-level robot prosthetic leg. The FSR sensor used in this study is RA9P (Marveldex). The response time is 10μs, the operating environment temperature is -20 to 60°C, the humidity is < 90%, and the durability is 2,000,000 cycles. Therefore, the robotic prosthetic leg is suitable for repeating walking motions in various environments. As for the FSR sensing result, we want the result obtained by contact recognition through pressure sensing, not accurate weight measurement. In this study, the FSR sensor is attached to the sole of the foot and recognizes the gait phase using information obtained when it contacts the ground. It is easy to use because it is not affected by the constitution of each patient and can be used without additional auxiliary equipment.

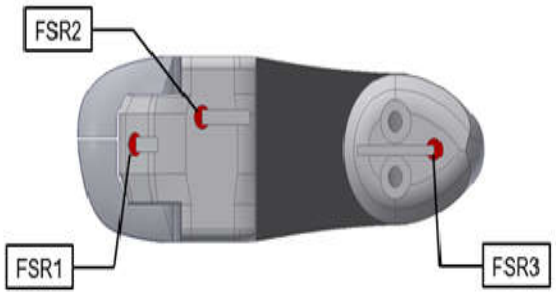

Fig. 5 FSR sensor foot-attachment location

The three FSR sensors are shown in Fig. 5. The sensor is located along the centerline of the pressure path generated on the sole by the movement of the center of gravity during walking [26-29]. FSR1 is attached to the slope of the metatarsal head, FSR2 to the front of the prosthesis, and FSR3 to the heel. FSR1 is not detected when standing attached to an inclined surface. FSR1 detects when the toes are bent from HO to TO and when the metatarsal heads touch the ground. This position distinguishes walking initiation after HO from simply lifting the foot. When FSR1 is activated, it means that the next gait is in progress, and the relay turns on the motor to operate plantar flexion. After TO, FSR1 is not detected, and toe clearance is made to prevent dragging of the foot to the ground during the swing phase by dorsiflexion. FSR3 is to distinguish between HS and HO phases. In the HS step, the FSR3 detects heel contact with the ground. At this time, the relay turns off the motor and plantar flexion is performed by weight movement. This saves energy consumption and relieves shock through the ankle and heel shock absorbers. FSR2 controls ankle rotation according to walking speed after FF. The walking speed is calculated by measuring the sensing time from FSR3 to FSR2, and the next motor operation time is adjusted.

EXPERIMENTAL ASSESSMENT

A. Evaluation of the walking-algorithm controller

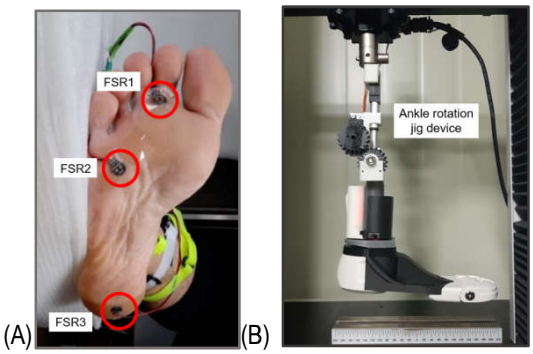

(A) (B)

Fig. 6 (A) FSR sensors attached to a human foot, and (B) the jig mounted for testing

To test the FSR control system, pressure change data obtained during walking were compared with human gait. The subject was a non-disabled adult male weighing 70 kg, and an FSR sensor was attached to the right foot as shown in Fig.6(A). The location of the FSR sensor was like that of the robotic prosthesis. The FSR attached to a person was selected along the line of the pressure path applied to the sole due to the shift of the center of gravity during walking. FSR1 was attached to the slope of the metatarsal head, FSR2 to the lateral surface of the forefoot, and FSR3 to the heel. FSR1 was attached to the metatarsal head for an effect like the inclined surface of a robot prosthesis, so that the pressure with the ground was not sensed when standing upright. The subject walked 4 times at a normal speed on a flat surface, and the pressure change with the ground from HS to was measured. As shown in Fig. 6(B), a device for walking with a prosthetic robot was fabricated and tested. It consists of a servomotor and a hydraulic cylinder to realize walking motion. Ground pressure change data was extracted using the FSR sensor on the sole.

B. Mechanical strength test

In this study, a robotic prosthetic foot was fabricated using Markforge's Onyx one 3D printer. Carbon fiber and nylon powder were used as substrates, and glass fibers were used as reinforcing fibers. To confirm whether the material can be used when introduced into the prosthetic leg, the physical properties of the material were measured using a universal tensile tester. The reference test method is ASTM D638. Table 3 is the material property data measured using a tensile tester. Finite element analysis was conducted using Autodesk's Inventor to prove that it could be used for prosthetic limbs based on the measured physical properties. The physical properties of the 3D printing material obtained through the tensile test were applied to the finite element analysis. The condition of this experiment is the TO situation in which the highest load is applied to the prosthetic foot of the robot while walking, assuming that a 70kg adult male wears it. Considering the safety factor, a load of 1.4 kN is applied to the slope of the metatarsal head, plantar flexion is performed by the motor, and it is set in a fixed state with the upper ankle part. The boundary condition is the ankle joint, more specifically, the plane where the leg part and the ankle part come into contact. Set the material's library element type to solid for precision. To increase reliability during the discretisation process, meshing was performed on the metatarsal slope and instep where the load is concentrated, and the number of nodes is set to 64,444 and the number of elements is set to 37,350. The numerical method of the prosthetic foot of the robot is analyzed and the von Mises stress

distribution and safety factor are derived to determine the safety according to the stress state. For these calculations, Inventor Professional 2022's ANSYS special module is utilized [30]. The factor of safety is the allowable stress divided by the actual stress. The actual stress is the von Mises stress, σ_{VM}, and the formula is Eq. (1)

$$\sigma_{VM} = \sqrt{\frac{1}{2}(\sigma_1 - \sigma_2)^2 + (\sigma_2 - \sigma_3)^2 + (\sigma_3 - \sigma_1)^2} \quad (1)$$

$\sigma_1, \sigma_2, \sigma_3$are the maximum principal stress, intermediate principal stress, and minimum principal stress. In the case of von Mises stress, it is a scalar value projected onto a tensile or compressive stress in one axis. When the prosthetic foot touches the ground, the weight load and the ground reaction force are parallel axes [31]. Therefore, it is judged that von Mises stress can be applied to the prosthetic foot of the robot.

TABLE III

MANUFACTURING MATERIAL PROPERTIES THROUGH TENSILE TESTING

Option	Value
Modulus of elasticity (*GPa*)	31.3
Shear modulus (*MPa*)	26.5
Compressive strength (*MPa*)	216.1
Tensile strength (*MPa*)	602.0
Density ($g \cdot cm^{-2}$)	1.5
Poisson's ratio	0.38

EXPERIMENTAL RESULTS

A. Algorithm-based gait phase recognition test result

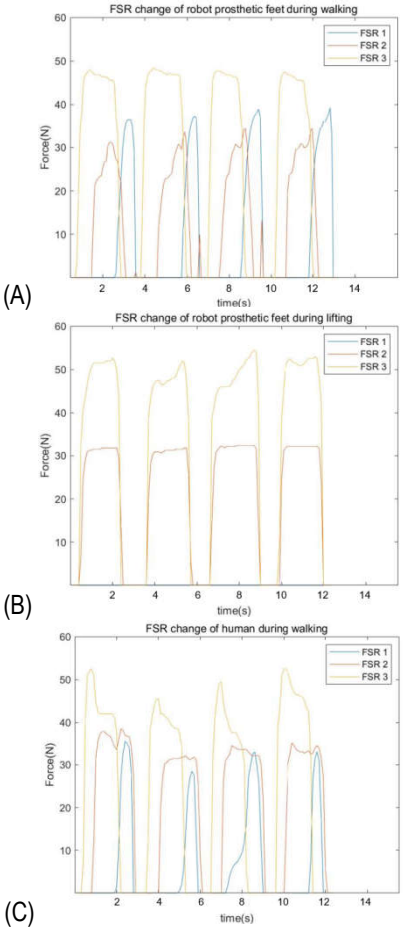

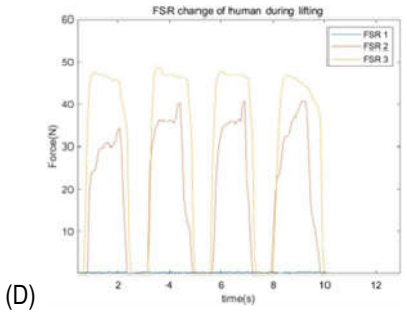

Fig. 7 FSR sensor foot-attachment location

As shown in Fig.7, it is a graph of the ground pressure change between the robot prosthetic leg and the sole of the human foot according to the gait stage. Fig. 7(A), (B) are walking of the robot prosthetic leg, (A) is walking from HS to, and (B) is simple lifting motion, not walking. Fig. 7(B), (D) are walking of the human, (C) is the walking from HS to, and (D) is a simple lifting motion, not walking. Each test involved 4 strokes with the right foot. In each graph, the x-axis represents time and the y-axis represents the pressure change (N) of the FSR. Comparing Fig. 7(A) and (C), it is the gait sensing result of the robot prosthetic foot and the human FSR sensor over time. FSR1, located at the metatarsal head, exhibits the same perceived motion time point from HO to for both human-robot prosthesis. The load applied to the FSR1 of the robot prosthesis is 38.34 N, and the load of the human is 27.16 N. This is because when the bent foot was formed after HO, the inclined surface of the metatarsal bone of the robot prosthesis was designed as a flat surface and a load was applied to the inclined surface. However, it is judged that there is a difference in value because the human foot is round, and the muscle tissue is deformed when a load is applied. However, as intended in this study, it means that the load after HO is supported by the slope of the metatarsal head. This can provide a more stable gait during the Double Support Pose when supported only by the toes. The red line, FSR2 located in the forefoot, sensed from FF to HO in the case of the robot prosthesis and from FF to in the case of the human foot. The reason for the different end time of FSR2 is that the prosthetic foot of the manufactured robot has a flat sole, whereas the human foot has a continuous curved surface. Additional research is needed to match the end points by rounding the sole of the robot prosthetic foot. Still, the starting point of FSR2 sensing of the robot prosthetic foot is always constant at about 2.4 seconds after the start of walking. Walking speed can be adjusted through motor control by detecting the start point of FF and calculating the time difference with FSR3.The yellow line, FSR3 located at the heel, showed the same detected motion points from HS to HO for both the robotic prosthesis and the human foot. Comparing Fig. 8(A) and (C), the sensing timing and the order of the moving center line of the two FSR sensors are similar. The gait phase can be sensed by the FSR sensing algorithm and appropriate ankle motion can be implemented with the motor. Comparing Fig. 7(B) and (D), both FSR2 and FSR3 are detected when the foot is in contact with the ground, and sensing is stopped when the foot is raised. FSR1 is located on the slope of the metatarsal bone and is not sensed because it is not in contact with the ground. However, FSR1 is detected in small amounts in humans. This is because, in the case of humans, the muscle tissue is deformed by the load while standing and the surface of the metatarsal bone touches the ground. In comparison, FSR1 of the prosthetic robot senses a value of 0 stably because it is located on the slope of the metatarsal head. This can prevent false detection of FSR1 and reduce gait classification errors.

B. Mechanical strength test result

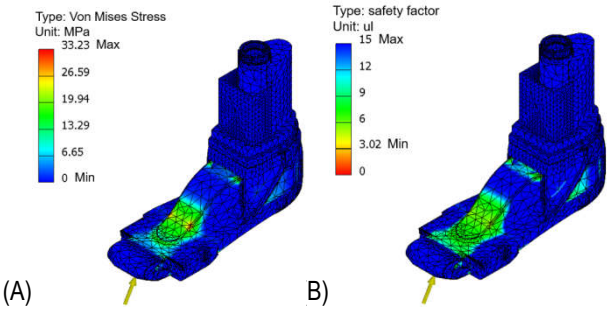

Fig. 8 Loading simulation results in TO. (A) von Mises stress (B) safety factor

The physical properties of the 3D printing material obtained through the tensile test were applied to the finite element analysis. Fig. 8(A) shows the simulation results for the robotic prosthetic foot. The distribution of internal stress due to the load applied to the slope is displayed as a color graph. The color distribution is classified into red and blue as shown in the color histogram on the left. Blue indicates a low failure probability due to internal stress and red indicates a high internal stress distribution. As a result of the experiment, the highest internal stress at 33.23 MPa was distributed in the instep area, and the internal stress was distributed in this area. Moments were generated on the inclined plane of the metatarsal head with applied load and the ankle axis with a fixed restraint. The red color indicates the possibility of fracture, but the tensile strength of the material used in this study was 602.0 MPa, which was higher than the maximum internal stress. Therefore, it was concluded that there was no fracture risk. Compared to other robotic prosthetic feet in which a load is applied to the tip of the toe, in this study, a bent shape is formed based on the axis of the toe and the load is applied to the slope of the metatarsal head. This shortens the displacement of the force point when the lever effect occurs based on the ankle axis, and a small moment is applied to the robot prosthetic foot. Additionally, Fig. 8(B) is a color graph that converts the safety factor into visual data. As the color goes red, the safety factor is less than 1, so the risk of breakage increases, and the more blue, the higher the safety factor. As a result of the experiment, the safety factor of the instep part was the lowest at 3.02. Because walking is performed repetitively according to the patient's physical condition in an unstructured environment, it is judged that a safety factor of 3 to 4 or more is necessary [32]. Therefore, it is judged that the materials used in this study can be used sufficiently for the robotic prosthetic foot. When looking at the stress distribution and safety factor results, it can be supplemented through design modification in future studies to prevent fractures caused by long-term repeated fatigue accumulation, given that stress is concentrated on the instep.

RESULTS

Fig. 9 The robotic prosthetic foot

In this study, to develop a bio-inspired and economical robotic prosthetic foot as shown in Figure 9, a specialized design and FSR sensor algorithm that integrates the toe joint and metatarsal head slope were used. A torsion spring was inserted between the toe and forefoot to form a curved foot shape from the HO to the toe axis. In TO, the elastic energy stored in the spring is released to provide propulsion to the wearer. After calculating the load applied to the toe as 82.32 N in the TO stage, an appropriate torsion spring was selected. In this study, the slope of the metatarsal head was designed, and the load was applied. The shift of the force point from the tip of the toe to the slope of the metatarsal head reduces the required strength and indicates that it can be manufactured using inexpensive materials. Physical property data were obtained through strength tests of the materials used, and the TO situation requiring the most load was implemented through 3D simulation. The highest stress part was 33.23 MPa and the tensile strength of the material used was 602.0 MPa, proving that the robot prosthetic foot could withstand it. The FSR sensor attached to the sole of the foot recognizes the wearer's gait phase, and the motor mounted on the ankle operates as desired. The robotic prosthetic leg was mounted on a jig and tested whether it could detect the start of walking, lifting, and walking speed. The FSR sensor was attached to the human foot at the same location as the robot prosthesis, and sensing was compared according to the gait stage. The sensing timing of the human and robot prosthetic limbs for each motion was similar, and it was shown that the FSR sensor algorithm proposed in this study can distinguish the gait phase. Each development has been used to reduce the cost of robotic prostheses and make them available to amputees and demonstrated their feasibility through strength and algorithmic controlled tests. The robotic prosthesis proposed in this paper can be manufactured using 3D printing technology and can be purchased for $500. In future studies, it will be necessary to develop a gait improvement function by inserting an encoder into the ankle axis motor to measure the rotation angle and feedback for gait data. In addition, additional research is needed to improve the design and increase the sensing sensitivity by implementing the curved surface of the human body and the arch of the foot.

REFERENCES

1. K. Z. Graham, E. J. MacKenzie, P. L. Ephraim, T. G. Travison, R. Brookmeyer,"Estimating the Prevalence of Limb Loss in the United States: 2005 to 2050,"Archives of PM&R, Vol. 89, No. 3, pp. 422-429, Mar. 2008, doi: 10.1016/j.apmr.2007.11.005.
2. M. Owings, and J. K. Lola, "Ambulatory and inpatient procedures in the United States 1996," No. 139. US Department of Health and Human Services, National Center for Health Statistics, 1998.
3. Y. Ogura et al., "Human-like walking with knee stretched, heel-contact and toe-off motion by a humanoid robot," in IEEE/RSJ International Conference on Intelligent Robots and Systems, Beijing, China, 2006, pp. 3976-3981.
4. C. K. Ahn, M. C. Lee, and S. J. Go, "Development of a biped robot with toes to improve gait pattern," in IEEE/ASME International Conference on Advanced Intelligent Mechatronics, Kobe, Japan, 2003, pp. 729-734.
5. C. McGreavy and Z. Li, "Reachability Map for Diverse and Energy Efficient Stepping of Humanoids," in IEEE/ASME Transactions on Mechatronics, vol. 27, no. 6, pp. 5307-5317, Dec. 2022, doi: 10.1109/TMECH.2022.3174961.
6. S. Kajita, K. Kaneko, M. Morisawa, S. Nakaoka and H. Hirukawa, "ZMP-based Biped Running Enhanced by Toe Springs," in IEEE International Conference on Robotics and Automation, Rome, Italy, 2007, pp. 3963-3969.

7. B. Henze, M. A. Roa, A. Werner, A. Dietrich, C. Ott and A. Albu-Schäffer, "Experiments with Human-inspired Behaviors in a Humanoid Robot: Quasi-static Balancing using Toe-off Motion and Stretched Knees," in International Conference on Robotics and Automation (ICRA), Montreal, QC, Canada, 2019, pp. 2510-2516,
8. Z. Huang et al. "Knee-stretched Walking with Toe-off and Heel-strike for a Position-controlled Humanoid Robot based on Model Predictive Control," IJ of Advanced Robotic Systems vol. 18, no. 4, Jul. 2021, doi: 10.1177/17298814211036282.
9. Y. Wu, Y. Pan, X. Leng, Z. He, "Kid-size robot humanoid walking with heel-contact and toe-off motion," PeerJ Computer Science, 7:e797, Mar. 2021, doi: 10.7717/peerj-cs.797.
10. Y. Chen, B. Xuan, Y. Geng, S. Ding and L. Chen, "Modeling and Control of Knee-Ankle-Toe Active Transfemoral Prosthesis," in IEEE Access, vol. 8, pp. 133451-133462, 2020, doi: 10.1109/ACCESS.2020.3010636.
11. L. Gabert, M. Tran and T. Lenzi, "Design of an Underactuated Powered Ankle and Toe Prosthesis," in 43rd Annual International Conference of the IEEE Engineering in Medicine & Biology Society (EMBC), Mexico, 2021, pp. 4920-4923, doi: 10.1109/EMBC46164.2021.9629842.
12. A. J. Hippolitus, A. Oberoi, "Design and Development of an IoT based Multi Terrain Humanoid Robot Foot," International Journal of MPERD, vol. 8, no. 6, pp. 143-150, Dec. 2018.
13. H. She, J. Zhu, Y. Tian, Y. Wang, Q. Huang, "Design of a powered ankle-foot prosthesis with an adjustable stiffness toe joint," Advanced Robotics, vol. 34, no. 10, pp. 689-697, Feb. 2020, doi: 10.1080/01691864.2020.1750479.
14. S. Agarwal and M. Popovic, "Study of Toe Joints to Enhance Locomotion of Humanoid Robots," in IEEE-RAS 18th International Conference on Humanoid Robots, Beijing, China, 2018, pp. 1039-1044, doi: 10.1109/HUMANOIDS.2018.8625052.
15. V. T. Nguyen et al., "Study of Bipedal Locomotion Considering Property of Toe Mechanism," in the 12th Asia Conference on Mechanical and Aerospace Engineering, online, 2022, Doi: 10.1088/1742-6596/2235/1/012068.
16. O. Eldirdiry and R. Zaier, "Modeling biomechanical legs with toe-joint using simscape," in 11th International Symposium on Mechatronics and its Applications (ISMA), Sharjah, United Arab Emirates, 2018, pp. 1-7, doi: 10.1109/ISMA.2018.8330129.
17. E. C. Honert, G. Bastas and K. E. Zelik, "Effect of toe joint stiffness and toe shape on walking biomechanics," Bioinspiration & Biomimetics, vol. 13, no. 6, Oct. 2018, doi: 10.1088/1748-3190/aadf46.
18. M. Sadedel, A. Yousefi-Koma, M. Khadiv, and F. Iranmanesh, "Heel-strike and toe-off motions optimization for humanoid robots equipped with active toe joints," Robotica, vol. 36, no. 6, pp. 925-944. Mar. 2018, doi: 10.1017/S0263574718000140.
19. E. Kouchak and A. Mokhtarian, "Controllability Analysis of a Standing Bipedal Robot with Active Toe-Joints," 2018 6th RSI International Conference on Robotics and Mechatronics, Tehran, Iran, 2018, pp. 343-348.
20. V. T. Nguyen and H. Hasegawa, "Effect of Toe Length on Biped Walking Behavior," International Journal of Mechanical Engineering and Robotics Research Vol. 7, No. 6, Nov. 2018, pp. 599-603, doi: 10.18178/ijmerr.7.6.599-603.
21. G. Bhardwaj, U. A. Mishra, N. Sukavanam and R. Balasubramanian, "Planning Adaptive Brachistochrone and Circular Arc Hip Trajectory for a Toe-Foot Bipedal Robot going Downstairs," International Conference on Robotics and Artificial Intelligence, Chennai, India, 2020, pp. 28-29.
22. U. Kanatli, H. Yetkin and S. Bolukbasi, "Evaluation of the transverse metatarsal arch of the foot with gait analysis," Arch Orthop Trauma Surg, vol. 123, Feb. 2003, pp. 148–150, doi: 10.1007/s00402-002-0459-7.
23. A. H. Shultz, B. E. Lawson and M. Goldfarb, "Variable Cadence Walking and Ground Adaptive Standing With a Powered Ankle Prosthesis," in IEEE Transactions on Neural Systems and Rehabilitation Engineering, vol. 24, no. 4, pp. 495-505, Apr. 2016, doi: 10.1109/TNSRE.2015.2428196.
24. M. K. Ishmael, D. Archangeli and T. Lenzi, "A Powered Hip Exoskeleton With High Torque Density for Walking, Running, and Stair Ascent," in IEEE/ASME Transactions on Mechatronics, vol. 27, no. 6, pp. 4561-4572, Dec. 2022, doi: 10.1109/TMECH.2022.3159506.
25. D. Tlalolini, C. Chevallereau and Y. Aoustin, "Human-Like Walking: Optimal Motion of a Bipedal Robot With Toe-Rotation Motion," in IEEE/ASME Transactions on Mechatronics, vol. 16, no. 2, pp. 310-320, Apr. 2011, doi: 10.1109/TMECH.2010.2042458.
26. H. Huber and M. Dutoit, "Dynamic Foot-Pressure Measurement in the Assessment of Operatively Treated Clubfeet," The Journal of Bone & Joint Surgery, vol. 86, no. 6, pp. 1203-1210, Jun. 2004.
27. K. Imaizumi, Y. Iwakami, M. Kumamoto, M. Tomisaki, M. Sudo and Y. Niki, "Evaluation of toe function based on the plantar pressure distribution while walking and its relationships with general gait parameters," 2019 41st Annual International Conference of the IEEE Engineering in Medicine and Biology Society (EMBC), Berlin, Germany, 2019, pp. 2434-2438, doi: 10.1109/EMBC.2019.8857454.
28. S. C. Ahn, S. J. Hwang, S. J. Kang and Y. H. Kim, "Development and evaluation of a new gait phase detection system using FSR sensors and a gyrosensor," Journal of the Korean Society for Precision Engineering, vol 21, no. 10, pp. 196-203, Oct. 2004.
29. S. J. M. Bamberg, A. Y. Benbasat, D. M. Scarborough, D. E. Krebs and J. A. Paradiso, "Gait Analysis Using a Shoe-Integrated Wireless Sensor System," in IEEE Transactions on Information Technology in Biomedicine, vol. 12, no. 4, pp. 413-423, Jul. 2008, doi: 10.1109/TITB.2007.899493.
30. Engineering ToolBox, (2010). Factors of Safety. [online] Available: https://www.engineeringtoolbox.com/factors-safety-fos-d_1624.html
31. H. J. Ahn, K. H. Lee, Y. Hong and C. H. Lee, "Design and Optimization of an Knee Joint of Fully-active Transfemoral Prosthesis for Stair Walking," Journal of rehabilitation welfare engineering & assistive technology, vol. 10, no. 1, (pp. 65-72, Feb. 2016.

AUTHORS BIOGRAPHY

Su Chak Ryu received the B.S. and Ph. D. degrees from Pusan University in 1986 and 1988, respectively. The departments of his B.S. and Ph. D. degrees were Ceramic Materials Engineering and Bio Materials Technology, respectively. He was recently appointed as a professor at the Department of Nanomechatronics Engineering in Pusan National University, Busan, Republic of Korea. His current research interests include bioengineering, and mechatronics.

Joon Hyub Kim received the B.S. and Ph. D. degrees from Korea University in 2009 and 2014, respectively. The departments of his B.S. and Ph. D. degrees were Control and Instrumentation Engineering and Bio Micro System Technology, respectively. He was recently appointed as a professor at the Department of Nanomechatronics Engineering in Pusan National University, Busan, Republic of Korea. His current research interests include MEMS-based sensors, nanobiosensors and environment sensor.

Sung Kwang Jo received the B.S. degree in nanomechatronics engineering from the Pusan national University, Pusan, Korea, in 2023. He is currently a master's course in nanomechatronics engineering at the Pusan national university, Pusan, Korea. His research interests include bioengineering, mechatronics.

Seung Hyeon Kim received his B.S. degree in nanomechatronics engineering from the Pusan National University, Pusan, Korea, in 2019. He is currently a master's course in nanomechatronics engineering at the Pusan National University, Pusan, Korea. His research interests include bioengineering, robot engineering, mechatronics, machinery, CAD/Inventor.

****